# A Damped Oscillation in the Intramembranous Charge Movement and Calcium Release Flux of Frog Skeletal Muscle Fibers

NATALIA SHIROKOVA, GONZALO PIZARRO, and EDUARDO RÍOS

From the Department of Physiology, Rush University School of Medicine, Chicago, Illinois 60612

ABSTRACT Asymmetric membrane currents and calcium transients were recorded simultaneously from cut segments of frog skeletal muscle fibers voltage clamped in a double Vaseline-gap chamber in the presence of high concentration of EGTA intracellularly. An inward phase of asymmetric currents following the hump component was observed in all fibers during the depolarization pulse to selected voltages ($\simeq -45$ mV). The average value of the peak inward current was 0.1 A/F (SEM = 0.01, $n$ = 18), and the time at which it occurred was 34 ms (SEM = 1.8, $n$ = 18). A second delayed outward phase of asymmetric current was observed after the inward phase, in those experiments in which hump component and inward phase were large. It peaked at more variable time (between 60 and 130 ms) with amplitude 0.02 A/F (SEM = 0.003, $n$ = 11). The transmembrane voltage during a pulse, measured with a glass microelectrode, reached its steady value in less than 10 ms and showed no oscillations. The potential was steady at the time when the delayed component of asymmetric current occurred. ON and OFF charge transfers were equal for all pulse durations. The inward phase moved 1.4 nC/μF charge (SEM = 0.8, $n$ = 6), or about one third of the final value of charge mobilized by these small pulses, and the second outward phase moved 0.7 nC/μF (SEM = 0.8, $n$ = 6), bringing back about half of the charge moved during the inward phase. When repolarization intersected the peak of the inward phase, the OFF charge transfer was independent of the repolarization voltage in the range −60 to −90 mV. When both pre- and post-pulse voltages were changed between −120 mV and −60 mV, the equality of ON and OFF transfers of charge persisted, although they changed from 113 to 81% of their value at −90 mV. The three delayed phases in

Address correspondence to Dr. E. Ríos, Department of Physiology, Rush University School of Medicine, 1750 Harrison Street, Chicago, IL 60612.

Dr. Shirokova's permanent address is A. A. Bogomoletz Institute of Physiology, Ukrainian Academy of Sciences, Bogomoletz St.4, 252601 GSP, Kiev 24, Ukraine.

Dr. Pizarro's present address is Departamento de Biofísica, Facultad de Medicina, Montevideo, Uruguay.

J. GEN. PHYSIOL. © The Rockefeller University Press · 0022-1295/94/09/0449/29 $2.00
Volume 104 September 1994 449–477

asymmetric current were also observed in experiments in which the extracellular solution contained $Cd^{2+}$, $La^{3+}$ and no $Ca^{2+}$. Large increases in intracellular [$Cl^-$] were imposed, and had no major effect on the delayed components of the asymmetric current. The $Ca^{2+}$ transients measured optically and the calculated $Ca^{2+}$ release fluxes had three phases whenever a visible outward phase followed the inward phase in the asymmetric current. Several interventions intended to interfere with Ca release, reduced or eliminated the three delayed phases of the asymmetric current. We conclude that these phases are capacitive, with no significant ionic component. All results could be well described by a model of EC coupling in which the oscillations of the asymmetric current are intramembranous charge movements, driven by changes in local voltage. In the model, the oscillations are the consequence of two feedback processes. One is positive: $Ca^{2+}$, released from the SR binds to a hypothetical site near the voltage sensors, increasing the local voltage. The other is the spontaneous inactivation of release, presumably also induced by $Ca^{2+}$, which reduces the local $Ca^{2+}$ concentration and the transmembrane voltage.

## INTRODUCTION

The mechanochemical reactions that generate contractile tension in muscle are triggered by an increase in myoplasmic [$Ca^{2+}$], due to release of calcium from the sarcoplasmic reticulum (SR). The $Ca^{2+}$ release SR channels are controlled by the potential across the T tubule membrane, in a process that involves voltage sensor proteins that are now thought to be the high affinity DHP receptors of the T tubule (Ríos and Brum, 1987; Tanabe, Takeshima, Mikami, Flockerzi, Takahashi, Kangawa, Kojima, Matsuo, Hirose and Numa, 1987; Tanabe, Beam, Powell, and Numa, 1988). Changes of these sensors driven by voltage underlie intramembranous charge movement (Schneider and Chandler, 1973).

Usually, the charge movement current in frog muscle has an early, exponential component, followed by a delayed hump, or Iγ (Adrian and Peres, 1977). $I_\gamma$ has attracted interest because it is extremely well correlated with $Ca^{2+}$ release, in timing, and in terms of voltage dependence and pharmacology (reviewed by Huang, 1989; Ríos and Pizarro, 1991). In recent work, an agreement has emerged on the existence of effects of $Ca^{2+}$ release and intracellular [$Ca^{2+}$] on charge movement (Csernoch, Pizarro, Uribe, Rodríguez, and Ríos, 1991; García, Pizarro, Ríos, and Stefani, 1991; Pizarro, Csernoch, Uribe, Rodríguez, and Ríos, 1991; Szucs, Csernoch, Magyar, and Kovács, 1991; Jong, Pape, and Chandler, 1992; Pape, Jong, and Chandler, 1992).

An important disagreement still remains, however. In the view of some researchers the delayed phases of charge movement involve a separate set of sensors (Huang, 1989; Hui and Chen, 1992), whose kinetics are altered by intracellular $Ca^{2+}$ (Pape et al., 1992). Pizarro et al. (1991) have proposed instead that the same set of EC coupling voltage sensors contribute to the early and delayed currents of charge movement, and that the late phases are due to local changes in membrane potential, caused by changes in local $[Ca^{2+}]_i$.

One key difference between these views is that the latter allows for the existence of changes in direction of charge movement during a depolarizing pulse, provided that the local potential fluctuates during the pulse. In the alternative view, that the delayed charge movement is carried by a different set of particles, driven by a

constant field, humps would be possible (Huang, 1989), but not the inward movement of charge. An inward phase in the asymmetric current was described by Pizarro et al. (1991) and similar phases have been seen in many other laboratories (García et al., 1991; Szucs et al., 1991; Heiny, Jong, Bryant, Conte-Camerino, and Tortorella, 1990). Hui and Chen (1994) also found an inward phase in asymmetric currents of frog muscle, but interpreted them as the result of a decaying intramembranous charge movement plus a slowly increasing outward ionic current.

In the present work we defined conditions in which the inward phases are large, and tested in many ways whether they are capacitive, or have ionic components.

We found a third phase in the asymmetric current, that follows the inward phase. We also found that these multiple phases in the asymmetric currents are in detailed correspondence with phases in the waveform of $Ca^{2+}$ release flux.

Simulations with a comprehensive model of EC coupling suggest that these oscillations of membrane current are intramembranous charge movements driven by changes in local voltage, and that these fluctuations are all manifestations of feedback between release channels and voltage sensors of EC coupling.

## METHODS

All studies were carried out on cut segments of fast twitch fibers from the semitendinosus muscle of the frog *Rana pipiens*, voltage-clamped in a double Vaseline gap. The design of the chamber, and techniques for dissection, voltage clamp, and measurement of membrane currents and calcium transients have been described in detail (Brum, Ríos, and Stefani, 1988*a*; Csernoch et al., 1991; González and Ríos, 1993). The fibers were slack, and the cut ends were permeabilized by exposure to saponin (Irving, Maylie, Sizto, and Chandler, 1987).

The voltage clamp circuitry was that introduced by Francini and Stefani (1989), which was found in recent work (González and Ríos, 1993) to improve the performance of the clamp of Kovács, Ríos, and Schneider (1983) in terms of clamp speed and noise in the currents. To check the performance of the clamp circuit, in six experiments the membrane potential was measured with a conventional micropipette connected to a high input impedance voltage-measuring circuit with capacitance compensation. The micropipettes were filled with internal solution 10 EGTA (Table I) and had a resistance between 10 and 40 MΩ. In some cases, the pipette also contained 10 mM $ClC_4$-, for testing the effect of intracellular application of $ClO_4$-. The presence of $ClO_4$- in the pipette did not appear to affect the fiber properties unless an injection was made. The ensuing effects will be dealt with elsewhere (Shirokova, N. R. Shirokov, and E. Ríos, manuscript In preparation).

Data were conditioned by 8-pole Bessel filtering at 2 kHz and acquired with a 16 bit D/A and A/D converter card (HSDAS 16, Analogic, Wakefield, MA) under a 386 based PC-compatible computer (CompuAdd Corp., Austin, TX). The data acquisition routines were generated by Drs. Ivan Stavrovsky and Miloslav Karhanek in our laboratory. The acquisition board sampled five channels sequentially at 200 kHz, then averaged five contiguous samples per channel to obtain four almost synchronous averages every 200 μs. These values were stored as records of 1,280 points (256 ms). Other frequencies and record durations were used, but not in the records shown.

Asymmetric currents were calculated conventionally, as differences between total current during test pulses and scaled currents during control pulses of 20 mV amplitude, starting from a subtracting holding level of −110 mV. The command pulses had their edges blunted by linear ramps, lasting 600 μs. The combination of these ramps and 16 bit data acquisition virtually eliminated the errors of subtraction that affected the early points of the transients in

our previous work. Records shown are without corrections unless stated otherwise. For computation of charge transferred, the transients of asymmetric current were integrated after subtraction of the steady level at the end of the pulse (no sloping baselines were used). The transients calculated in this way are termed charge movement currents, or $I_Q$, only after the section of Results where we give evidence on their nature.

The internal solution contained in all experiments the dye antipyrylazo III (ApIII). The time course of change in free $[Ca^{2+}]_i$ was derived from the changes in absorbance at 720 and 850 nm (Brum et al., 1988*a*). The time course of $Ca^{2+}$ release flux from the SR was estimated from measured $\Delta[Ca^{2+}](t)$ by the method described by Brum, Ríos, and Schneider (in Brum et al., 1988*a*, Appendix). The method involves the fitting of a model of removal of $Ca^{2+}$ from the cytoplasm to the measured decay of $[Ca^{2+}]_i$. González and Ríos (1993) considered advantages and disadvantages of this technique, concluding that the time course of the calculated waveform of release is robust, in the sense that it is essentially independent on the assumptions regarding the removal processes, provided that the measured $Ca^{2+}$ transients are well fitted by

TABLE I

*Solutions*

| | Internals | | | Externals | |
|---|---|---|---|---|---|
| | *10 EGTA* | *20 Cl* | *50 Cl* | *10 Ca* | *10 Mg* |
| ApIII | 0.8 | 0.8 | 0.8 | — | — |
| ATP | 5 | 5 | 5 | — | — |
| Ca | * | * | * | 10 | 10 |
| Cl | 0 | 10 | 50 | — | 20 |
| Cs | 125 | 125 | 125 | — | — |
| $CH_3SO_3$ | — | — | — | 130 | — |
| EGTA | 10.4 | 10.4 | 10.4 | — | — |
| Gluconate | — | — | — | — | 110 |
| Glutamate | 100 | 80 | 50 | — | — |
| Mg | 5.5 | 5.5 | 5.5 | — | — |
| TEA | — | — | — | 122.5 | 122.5 |

All concentrations are in millimolar.

*The internal solutions had calcium added for a nominal $[Ca^{2+}]$ of 20 nM. All internal solutions had 5 mM phosphocreatine and 5 mM glucose. All external solutions had 1 μM TTX, 1 mM 3,4 diaminopyridine and 1 mM 9-anthracene carboxylic acid. All solutions had 10 mM HEPES and were titrated to pH 7.0 at room temperature.

the removal model (a similar conclusion had been reached before by Schneider, Ríos, and Melzer, 1987). This is particularly true when the internal medium contains a high [EGTA], as the time course of the $Ca^{2+}$ transients becomes very similar to that of the computed $Ca^{2+}$ release flux. Kinetic features of the release flux that are newly described in this paper, are also found in the $Ca^{2+}$ transients, and therefore are unlikely to be a spurious consequence of the analysis.

The fitting procedure started with a standard set of values of the parameters, then an iterative routine changed some of the parameters until a best (in the least squares sense) combination of new values was found. In the present paper, the parameters that were changed in the fitting procedure were [EGTA], its rate constants of $Ca^{2+}$ binding and unbinding, and the maximum pump rate at saturating $[Ca^{2+}]$. The other parameters were set to the same value in all records shown, as follows: $k_{OFF\ Ca\ Trop}$, 1,200 $s^{-1}$; $k_{ON\ Ca\ Trop}$, 125 $\mu M^{-1}\ s^{-1}$; $k_{ON\ Ca\ Parv}$, 100 $\mu M^{-1}\ s^{-1}$; $k_{ON\ Mg\ Parv}$, 0.03 $\mu M^{-1}\ s^{-1}$; $k_{OFF\ Ca\ Parv}$, 1 $s^{-1}$; $k_{OFF\ Mg\ Parv}$, 3 $s^{-1}$; $K_{D\ pump}$, 1 μM; [pump $Ca^{2+}$-binding sites], 100 μM; [parvalbumin], 1 mM; [troponin], 240 μM; $[Mg^{2+}]$, 900 μM. The

removal model was also a component of the model of EC coupling presented in the Discussion. In model simulations (Figs. 16–18), the standard parameter values, listed above, were used, plus 10 mM for [EGTA], 1 $\mu M^{-1}$ $s^{-1}$ and 1 $s^{-1}$ for the rate constants of EGTA:Ca, and 1.2 mM $s^{-1}$ for the maximum pump rate.

*Solutions.* They are detailed in Table I. The external solution 10 Ca was used in general. In two experiments we used 10 Mg, in which the main anion is gluconate. This solution is similar to one reported by Chen and Hui (1991) to increase the relative contribution of $Q\gamma$ to the charge transfer. The osmolality of the internal solutions was adjusted to 0.26 osmol/kg and that of the extracellular solutions to 0.27 osmol/kg. The temperature was 12°C.

## RESULTS

### *An Inward Phase of Asymmetric Current Appears in All Experiments*

An inward phase was observed at selected voltages in all fibers prepared in the same way. Fig. 1 displays asymmetric currents in ten consecutive experiments (#1062 and

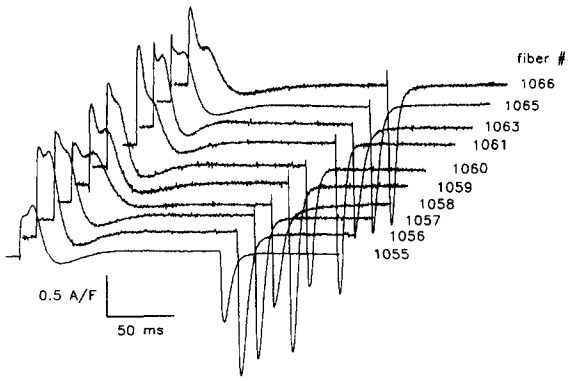


FIGURE 1. Presence of delayed components of the asymmetric current in 10 consecutive experiments. Test pulses from pedestal −60 mV were applied to −45 mV for fibers ## 1055, 1063, 1065, 1066, to −40 mV for # 1060 and to −35 mV for ## 1056, 1057, 1058, 1059, 1061. External solution was 10 Ca and internal solution was 10 EGTA in all experiments. Linear capacitances were between 18.5 and 25 nF. All fibers were at slack length.

1064 were unstable and were discarded). The voltages at which the records were obtained are the ones that elicited the clearest inward phase; they varied within 10 mV and are listed in the legend. The average value of peak inward current in 18 experiments was 0.10 A/F (SEM = 0.01) and the time at which the peak occurred was 34 ms (SEM = 1.8).

An additional, obvious observation is that all traces in the figure had a visible "hump" of $Q\gamma$. This was generally the case for fibers having a marked inward phase.

An unexpected observation was made: in almost every case, a third delayed phase, this one outward, was noticed after the inward phase. This phase was smaller, of less than 0.05 A/F, peaked at a more variable time (between 60 and 130 ms) and in many cases could only be separated from the final level if pulses of 150 ms or longer duration were applied.

The three delayed phases of the asymmetric current will henceforth be termed "hump," "inward," and "second outward." We avoid the further use of greek

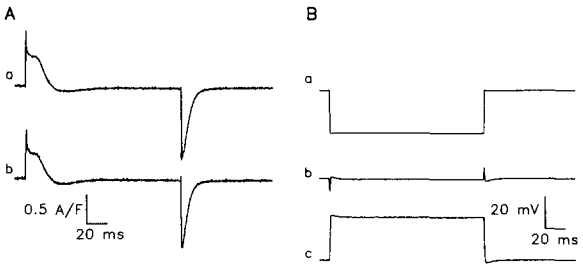


FIGURE 2. Asymmetric current and transmembrane voltage. (*A*) Asymmetric currents obtained from a slack fiber, voltage clamped in a double Vaseline gap, before (*a*) and after impaling the fiber with a glass microelectrode (*b*). Test pulse applied from −75 mV to −45 mV. (*B*) Voltage records obtained with microelectrode: (*a*) voltage in the bath; (*b*) voltage measured after impalement; (*c*) difference *a–b*, the transmembrane voltage. Fiber: #1065, linear capacitance: 18.5 nF, diameter: 148.8 μm.

subindicies as we will argue that all these phases probably obey the same mechanism, and should therefore be considered as part of the delayed current $I\gamma$.

To ascertain the performance of the voltage clamp circuit, we measured directly the imposed transmembrane voltage in five fibers, using a glass micropipette. Records from a representative experiment are in Fig. 2. The traces in Fig. 2 *A* are records of asymmetric current, obtained before (*a*) and after (*b*) impaling the fiber with the micropipette, at a voltage eliciting inward phases. It is clear that the impalement had no consequences for the Vaseline gap current measurements. The records in *B* were obtained with the microelectrode: *a* is the voltage in the bath, when a 30-mV pulse was applied before impalement (in this clamp device pulses are applied to the bath, inverted). *b* is the corresponding voltage after impalement. The circuitry clamps the intracellular compartment to ground, and what is recorded is the difference between the actual voltage and the desired zero. *c* is the difference $b - a$, the applied transmembrane voltage. In this and all other analogous experiments, the potential reached its desired steady value in less than 10 ms, and showed no

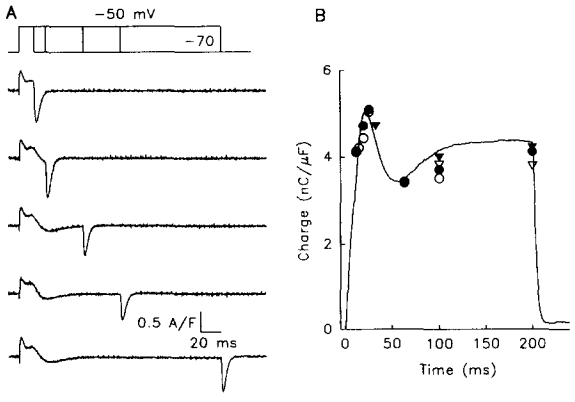


FIGURE 3. Conservation of charge in the delayed phases of the asymmetric current. (*A*) Asymmetric currents evoked during pulses of different durations, shown without correction. (*B*) Comparison of the time integral of the asymmetric current elicited by the 200-ms pulse (*line*) with the charge carried during the OFF of the various pulses (*symbols*). Different symbols represent different repetitions of the set of durations. The base line for the calculation of the ON integral was the average of the last 30 ms of the asymmetric current. No sloping base line correction was done. Fiber: #950, linear capacitance: 25 nF, diameter: 166.7 μm.

oscillations or ON/OFF asymmetries. The measured membrane potential was steady at the time of the main delayed phases of the asymmetric current.

*The Delayed Charge Returns at the OFF*

In a conventional test that these phases of asymmetric current are capacitive, we performed, in many fibers, the measurements represented in Fig. 3. At a voltage eliciting a marked inward phase, pulses of different duration were applied. The durations were chosen carefully to intersect: the peak of the hump, the end of the hump and beginning of the negative phase (duration 1 in Table II), the end of the inward phase (duration 2), and a duration greater than the end of the second

TABLE II

*ON and OFF Charges Transferred during the Late Phases of $I_Q$*

| Fiber | $V_{pre}$ | $V_{test}$ | $C_M$ | $Q_{OFF_1}$ | $Q_{OFF_2}$ | $Q_{OFF_3}$ | $\Delta_1$ | $\Delta_2$ | $\Delta_3$ |
|---|---|---|---|---|---|---|---|---|---|
| ## | *mV* | | *nF* | | | *nC/μF* | | | |
| 945 | −60 | −35 | 25.7 | 6.15 | 5.22 | — | 1.24 | 1.28 | — |
| | | | (0.7) | — | (0.1) | | | | |
| 950* | −85 | −65 | 27.5 | 6.6 | 4.75 | — | 0.03 | −0.35 | — |
| | | | (0) | (2.7) | (0.2) | | | | |
| 950 | −70 | −50 | 32.4 | 6.51 | 3.98 | 6.14 | 2.43 | −0.32 | 1.66 |
| | | | (0.6) | (0.5) | (0.6) | (—) | | | |
| 951* | −90 | −70 | 26.7 | 6.18 | 5.39 | 5.58 | 0 | −0.63 | −0.67 |
| | | | (0.3) | (0.07) | (—) | (—) | | | |
| 959 | −70 | −50 | 25 | 5.06 | 3.42 | 4.06 | 0 | 0.01 | 0.33 |
| | | | (0.9) | (0.02) | (0.02) | (0.13) | | | |
| 960 | −70 | −50 | 17.8 | 3.66 | 2.81 | 3.25 | −0.06 | 0.17 | 0.4 |
| | | | (0.5) | (0.04) | (0.03) | (0.08) | | | |
| 961 | −75 | −65 | 15.1 | 3.62 | 2.79 | 3.24 | −0.28 | 0 | 0.7 |
| | | | (0.1) | (0.05) | (0.12) | (0.4) | | | |
| Average | | | | 5.4 | 4.05 | 4.72 | 0.48 | 0.02 | 0.36 |
| SEM | | | | (0.5) | (0.56) | (0.56) | 0.38 | 0.23 | 0.37 |

Pulses are from the $V_{pre}$ level to $V_{test}$. $Q_{OFF_j}$ is OFF charge transfer, after pulses of three durations: $j = 1$ intersects the start of the inward phase (≃25 ms), $j = 2$ the end of the inward phase (≃55 ms) and 3 is the longest pulse (150 or 200 ms). $\Delta_j$ values are differences between the OFF values listed and ON values at the same duration, calculated on the asymmetric current obtained with the longest pulse. The averages of these paired differences are not significantly different from zero (two-tailed $t$ test).
External solution for the fibers indicated by * was 10 Mg, for all others 10 Ca.

outward phase. A long duration pulse (duration 3 in Table II, usually 200 ms) was also applied, to determine the baseline of the asymmetric current.

Fig. 3 *B* represents as a continuous record the time integral of the current transient during the longest pulse. The symbols represent the charge carried during the OFF of the various pulses. The sequence of pulses of different duration was repeated four times and four kinds of symbols represent the values in the four repetitions. The agreement between $Q_{ON}$ and $Q_{OFF}$ was good at all durations.

Six fibers were studied in approximately the same manner and the results are summarized in Table II. To maximize the proportion of slowly moving charge, the test pulse was applied in most cases from a prepulse level 15–40 mV depolarized

from the holding potential. Both pre- and test pulse levels are indicated. The table lists for each experiment six values of charge. $Q_{OFF_1}$, $Q_{OFF_2}$ and $Q_{OFF_3}$ are the charges moved during the OFFs of pulses of three durations (defined before); $\Delta_1$, $\Delta_2$, and $\Delta_3$ are the differences between the $Q_{OFF_j}$ and charges moved during the ONs at the corresponding durations (measured on the record obtained with the longest pulse). These paired differences between ON and OFF transfers were not significantly different from zero.

In most experiments the external solution was 10 Ca; in #951 it was 10 Mg (in which the main anion is gluconate) and in experiment #950, one run was done in each solution. Data with both solutions are listed. The asymmetric currents showed all delayed phases with both solutions. The only obvious difference observed in 10 Mg was a shift in the voltage dependence of activation to more negative potentials, the most apparent negative phase was recorded at or near −45 mV in 10 Ca and at −65 mV in 10 Mg. A corresponding shift was observed in the measurements of $Ca^{2+}$ transients and release, to be described later.

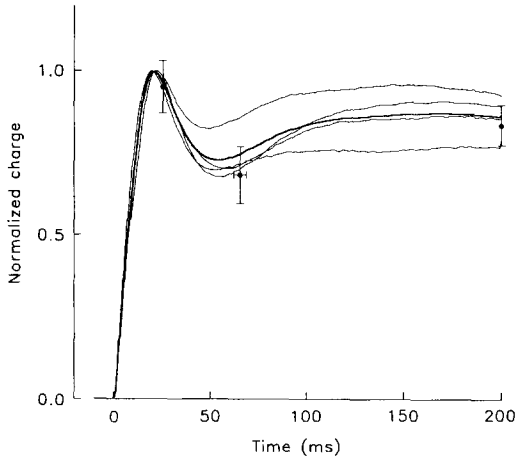


FIGURE 4. Comparison of ON and OFF charges in four identically prepared fibers. Thin lines are the individual running integrals for a pulse to −50 mV (for fibers ##950, 959, 960) or to −65 mV (for fiber #961), which were normalized to the maximum value for each fiber separately. The thick line is their average. The symbols represent the normalized and averaged OFF areas for the test pulse durations 1, 2, and 3, corresponding to the beginning and the end of the inward phase and to the longest duration. Normalization values (in nanocoulomb/microfarad): #950, 8.9; #959, 5.1; #960, 3.6; #961, 3.3.

Another comparison is shown in Fig. 4, representing runs in four identically prepared fibers (the two other fibers in Table II were not included because a 200-ms pulse was not applied). The integrals of transients for the longest pulses (200 ms) are represented by thin traces. Each record is scaled to the value of their early maximum. The OFF charges at times 1, 2, and 3 were normalized to the individual maximum of the integral, and averaged. The symbols represent the averages and the bars are SEM.

The sum of the evidence in this section indicates: (*a*) that there is essential equality between ON and OFF values at all durations, consistent with a capacitive nature of the current; (*b*) that the inward phase moves some 1.5 nC/μF of charge, or about one third of the final value of charge mobilized by these small pulses; and (*c*) that the second outward phase moves ~0.7 nC/μF, bringing back about half of the charge moved during the inward phase.

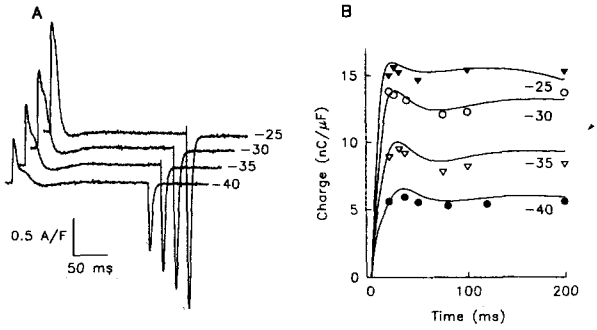


FIGURE 5. Voltage dependence of the delayed components. (*A*) Asymmetric currents elicited by the test pulses to the voltages indicated. (*B*) The comparison of their time integrals after subtracting a horizontal level (*lines*) with OFF charges calculated from the pulses of different durations (*symbols*). Fiber: #1059; linear capacitance: 20.5 nF; diameter: 101.2 μm.

*The Inward Phase Appears in a Narrow Voltage Range*

Typically, the inward phase and the 2nd outward phase are clear in a 20-mV range. Fig. 5 illustrates a representative experiment, in which the inward phase was noticeable only in the range covered by the records shown. The records are uncorrected asymmetric currents. The continuous curves in Fig. 5 *B* are their integrals after subtracting a steady level, and the symbols are OFF charges in pulses of equal or shorter duration. The general equality remarked earlier is also found here. The data illustrate that the inward current moves a maximum amount of charge in the center of the range. Similar observations of detailed agreement of ON and OFF charge at different voltages were made in three experiments.

*The Inward Phase at Different Driving Forces*

An additional test of the nature of the inward current is illustrated in Fig. 6. At a voltage where a sizable inward current was recorded, the duration intersecting the peak was determined. Then pulses of this duration were applied with the pattern shown, changing the return voltage, so that the OFF current moved under different driving forces. If the inward phase corresponded to an ionic current activated during the pulse, one would predict that the OFF "tail" would increase as the OFF voltage was made more negative, and the charge moved would increase accordingly. The OFF charge, computed directly on the asymmetric currents is represented by filled

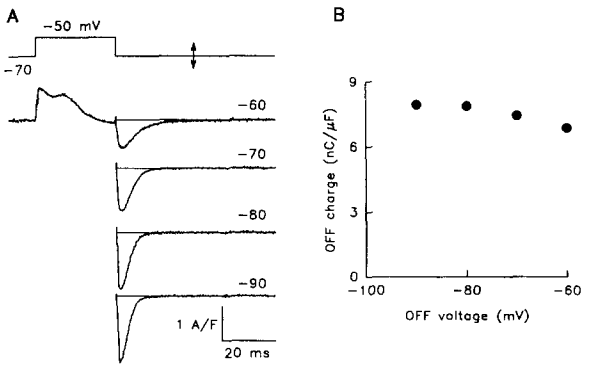


FIGURE 6. Asymmetric currents at different driving forces. (*A*) Asymmetric currents recorded at different OFF voltages. The thin lines mark the average level of the last 25 ms. (*B*) OFF charge transfer vs return voltage. Fiber: #950; linear capacitance: 25 nF; diameter: 166.7 μm.

circles in *B*. The reference level was the average of the last 25 ms of the OFF current. In this experiment, the OFF charge essentially did not change at the potentials explored. This is consistent with a capacitive charge whose voltage dependence is minimal below −60 mV. It would be consistent with an ionic current only if the kinetics of deactivation at negative voltages accelerated in such a way as to exactly compensate for the increase in driving force, so that charge transfer remained constant. This type of experiment was repeated in three fibers, with similar results.

With a similar rationale we devised a variant of the experiments of the previous section. In this variant both the prepulse level and the OFF or postpulse level were changed in parallel, while the test level was kept constant, at a value that gave substantial inward phase. As in the previous experiment, the OFF intersected the

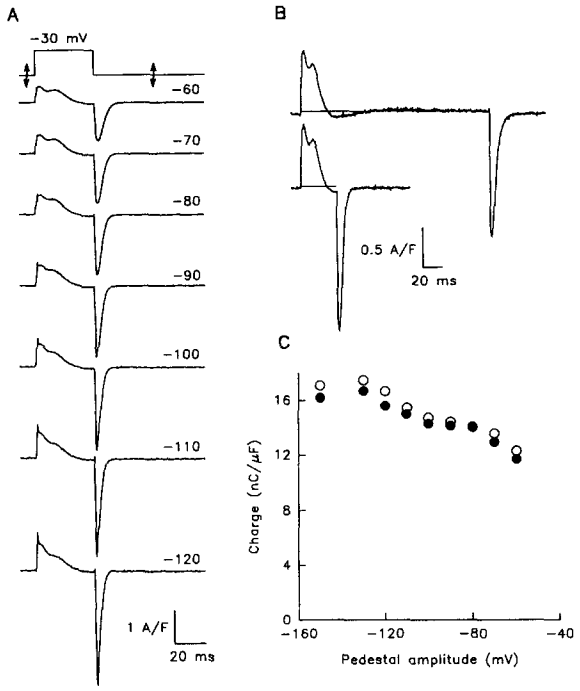


FIGURE 7. ON and OFF charge transfers at different pre- and post-pulse voltages. (*A*) Asymmetric currents for pulse to −30 mV, from "pedestal" voltages indicated. The duration was such that the OFF intersected the maximum inward current. (*B*) A long pulse applied at every pedestal voltage to determine a horizontal baseline. This record was used for calculation of the ON charge in the short pulse. (*C*) ON and OFF charges vs pedestal voltage. Fiber: #1059; linear capacitance: 20.5 nF; diameter: 101.2 μm.

maximum of inward current. Fig. 7 illustrates the asymmetric currents (*A*) and charges (*C*) in one of six similar experiments. Shown in *B* are the asymmetric current during a long pulse, used at every prepulse level to determine a horizontal baseline to compute ON charge, and the short pulse, intersecting the peak of the inward phase, used to compute OFF charge. One advantage of this pattern is that it allowed us to compare directly ON and OFF charges, which are expected to be equal only if no ionic currents activate (or deactivate) during the ON. As the plot shows, the charges are similar at all voltages, though not constant. The amounts vary with pedestal level in an interesting manner, decaying sharply as the level increases above −70 mV (presumably because the prepulse invades the range of steep distribution of charge 1) and increasing somewhat when the prepulse is made more negative than

−100 mV (probably a result of simultaneous reductions of charge 2 and charge moving under the Vaseline seals, as discussed by Ríos and Pizarro, 1991). The main observation, however, is that ON and OFF charges changed in parallel, consistent with a purely capacitive inward phase.

The experiment was repeated in four fibers. As the prepulse voltage was changed between −120 mV and −60 mV, the ON charge was reduced from 113% to 83% of its value at −90 mV, and the OFF charge was reduced from 113 to 79% of its value at −90 mV. The similar reduction in ON and OFF by the increase in prepulse level is inconsistent with an ionic current that activates during the ON.

*Chloride Currents Do Not Contribute to the Inward Phase*

Given the composition of the solutions it is extremely unlikely that an inward movement of cations contribute significantly to the inward phase. All solutions contained TTX, 3–4 DAP, and no alkali metal ions. The inward phase had similar properties whether the external solution was 10 Ca or 10 Mg.

Moreover, substantial inward phases were found in the presence of Cd and La as sole extracellular inorganic cations. An example is in Fig. 8: the internal solution was

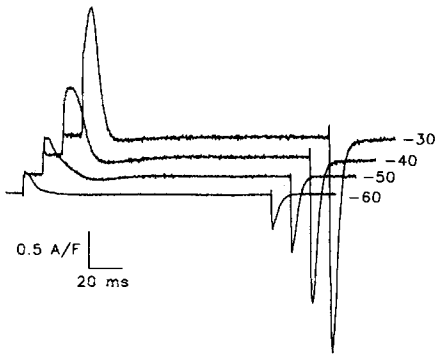


FIGURE 8. Asymmetric currents in the absence of extracellular $Ca^{2+}$. Test-minus-control currents, not corrected for sloping or steady baselines, elicited by 150 ms pulses to the voltages indicated. The external solution was Cd-La-A9C (Csernoch et al., 1991), similar to 10 Ca, but with 2 mM $Cd^{2+}$ and 0.1 mM $La^{3+}$ instead of $Ca^{2+}$. Internal solution, 10 EGTA. Fiber: #1085; linear capacitance: 18.5 nF; diameter: 95 μm.

10 EGTA, but the external solution was the one termed Cd-La-A9C by Csernoch et al. (1991). Delayed inward and outward phases are present in the asymmetric currents (shown without correction), with all the characteristics described for the experiments in 10 Ca (Fig. 1). The voltage dependence of the late phases is similar to the one described earlier (Fig. 5) and is also against the possibility that the inward phase is carried by cations through voltage-dependent Ca channels. The delayed phases, however, were smaller and less sharply defined, in this and other experiments with Cd-containing solutions. Experiments like this one justify our use of 10 Ca as the external solution of choice for the study of the delayed asymmetric current phases.

Next, we considered whether ions in the internal solution contribute to the inward phase. The possibilities include an inward current carried by an outward flux of anions or a delayed outward current carried by intracellular cations. The last is improbable as $Cs^+$ was the main intracellular cation. Even though the internal solutions contained little or no $Cl^-$, we directly tested the possibility of a $Cl^-$ contribution, which might occur for instance if the intracellular compartment did not equilibrate readily with the solution in the end pools.

The tests consisted in changing the internal solutions to others with high [$Cl^-$]. Fig. 9 represents one of two similar experiments. After recording charge movement current with a substantial inward phase (reference), the internal solution in the end pools was changed to 20 Cl. Shown are uncorrected asymmetric currents, recorded at the time indicated after solution change. 40 min after the change, the solution was changed back to 10 EGTA and more records were obtained (washout). Fig. 9 *B* shows superimposed the reference (*thin line*), washout (*thick line*) and the record obtained after 24 min in 20 Cl (*dotted*). The inward phase was similar in all records, even though an asymmetric inward current appeared, apparently with an instantaneous plus a slowly activating component. More charge moved in the controls (*C*), an observation for which we do not have a good explanation.

In two additional experiments, one of which is illustrated in Fig. 10, a 50 Cl internal solution was used instead. This solution caused a large increase in holding

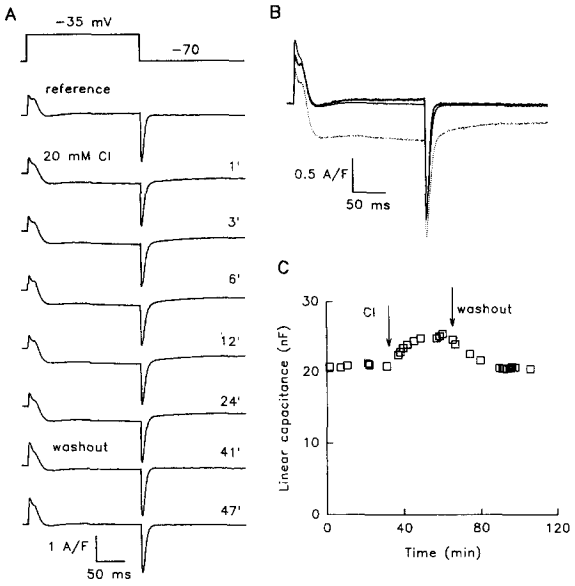


FIGURE 9. Effect of 20 mM intracellular $Cl^-$ on delayed components of the asymmetric current. (*A*) Asymmetric currents elicited by a pulse to −35 mV in internal solution 10 EGTA (reference), in 20 Cl, and after washout. The times after changing the internal solution to 20 Cl are indicated. (*B*) Superimposed reference (*thin trace*), washout (*thick trace*), and one record obtained after 39 min in 20 Cl (*dotted*). (*C*) Capacitance evaluated in the control pulses. Arrows mark the times of solution changes. Fiber: #1029; diameter: 97.6 μm.

current. To reduce somewhat the current we reduced the holding potential from −100 mV to −90 mV for the time the fibers were exposed to high $Cl^-$ internally, and the reduced holding potential was kept some time after washout. Despite major changes in holding current, and the development of a large inward asymmetric current, the hump and inward phase in the records were quite conserved during the intervention.

*Correspondence between Charge Movement and Ca Release Flux*

The change in intracellular [$Ca^{2+}$] was monitored in these experiments with the dye ApIII. From the Δ[$Ca^{2+}$] transients, the release flux $\dot{R}(t)$ was derived. Since we started from $Ca^{2+}$ transients obtained in the presence of a high concentration of EGTA, most of the features that will be described in the release flux are already present in the

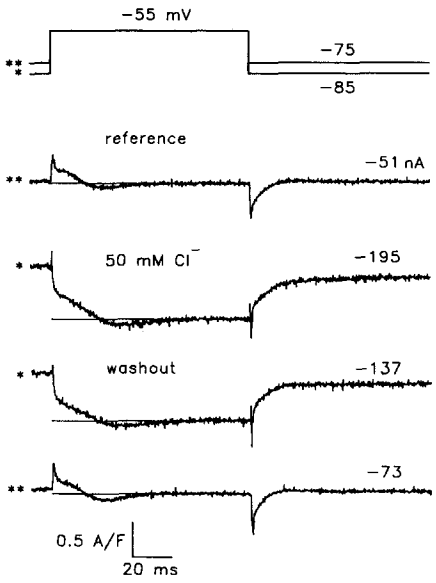


FIGURE 10. Effect of high intracellular $Cl^-$ concentration on asymmetric currents. Records obtained in internal solution 10 EGTA, 8 min after changing internal solution to 50 Cl and 2 and 31 min after washout. Extracellular solution 10 Mg. The holding potential was −100 mV and was changed to −90 mV in 50 Cl. The pedestal potential was also changed by −10 mV. Fiber: #953; diameter: 159 μm; linear capacitance was changed from 31 nF in 10 EGTA to 36 nF in 50 Cl and 31 nF after washout.

$Ca^{2+}$ transients, which makes the qualitative observations essentially independent of the assumptions used to derive the release waveform (Ríos and Pizarro, 1991).

A substantial and detailed correspondence between phases in release flux and in charge movement current ($I_Q$) was observed in all cases, and is illustrated in Fig. 11. The peak of release occurs somewhat later than the hump of $I_Q$, then release decays but, instead of remaining steady at the minimum value as described in the literature (Melzer, Ríos, and Schneider, 1984; Schneider, Simon, and Szucs, 1987; Schneider

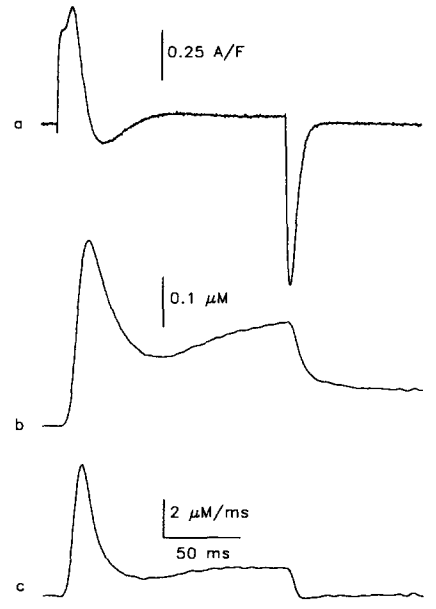


FIGURE 11. Asymmetric current and $Ca^{2+}$ release. Asymmetric current (*a*), $Ca^{2+}$ transient (*b*) and calculated release flux (*c*), for a 150 ms pulse from −60 to −45 mV. Fiber: #1055; linear capacitance: 22 nF; diameter: 107.1 μm. Parameters of removal (in addition to ones that were listed in Methods): [EGTA], 7.5 mM; $k_{ON\ Ca\ EGTA}$, 1.6 $\mu M^{-1}\ s^{-1}$; $k_{OFFCa\ EGTA}$, 4.5 $s^{-1}$; maximum pump rate; 1 mM $s^{-1}$.

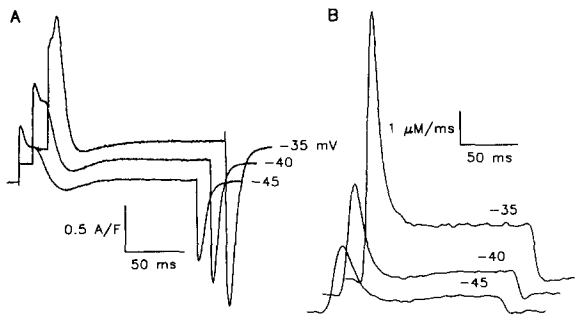


FIGURE 12. Voltage dependence of the delayed phases of $I_Q$ and release flux. (*A*) Charge movement recorded at test voltages indicated. (*B*) Release fluxes, calculated from the $Ca^{2+}$ signals measured simultaneously with the current traces shown in *A*. Fiber: #1056; linear capacitance: 20 nF; diameter: 107.1 μm. Parameters of removal: [EGTA], 8 mM; $k_{ON\,Ca\,EGTA}$, 1.6 $\mu M^{-1}\ s^{-1}$; $k_{OFF\,Ca\,EGTA}$, 3.6 $s^{-1}$; maximum pump rate: 4 mM $s^{-1}$.

and Simon, 1988; Brum et al., 1988; Simon, Klein, and Schneider, 1991) it goes through a minimum and then recovers somewhat before reaching a steady level. These three-phase kinetics were present in the release records every time a visible outward phase followed the inward phase in $I_Q$.

Fig. 12 demonstrates that the exquisite voltage dependence of the inward and late outward phases of $I_Q$ are also present in the release flux. The set of simultaneous records illustrate in particular the close association between the second outward phase in $I_Q$ and the second rise in $\dot{R}(t)$.

The temporal relationships between the different phases of release flux and $I_Q$ were also reproducible. They are illustrated in Fig. 13. As first shown by Csernoch et al., (1991) the phases in $I_Q$ bear a simpler relationship with $\dot{R}(t)$ (the time derivative of the release flux) than with $\dot{R}(t)$. This observation is now extended to the later phases. The apex of the hump in $I_Q$ is contemporal with the positive extreme of $\dot{R}(t)$. The negative extreme of $\dot{R}(t)$ clearly precedes (and is more marked than) the minimum of $I_Q$. Additionally, $\dot{R}(t)$ has a late positive phase that appears to be cotemporal with the second outward phase of $I_Q$. The precision of either measurement is not enough to rule out differences in timing of 20 to 30 ms between the late positive phases.

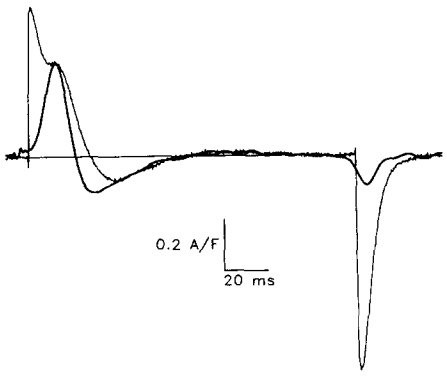


FIGURE 13. Timing comparisons. Superimposed are $I_Q$ for a pulse to −45 mV (Fig. 11 *A*) and derivative of the release flux calculated from the corresponding trace in Fig. 11 *B*, scaled to match its peak with the hump of $I_Q$. Fiber: #1056.

More evidence of close association between release flux and the various phases of asymmetric current was obtained with interventions that interfere with $Ca^{2+}$ release or the $Ca^{2+}$ transient.

First, we applied conditioning by a large pulse ("protocol 1" in Csernoch et al. [1991], García et al. [1991] and Szucs et al. [1991]). As shown in Fig. 14, a 90-ms conditioning pulse to 0 mV causes a selective reduction in the inactivating component of release flux during a test to −50 mV (*B*), suppression of hump and inward phase (*A*), and complete elimination of the second delayed component of asymmetric current (*A*).

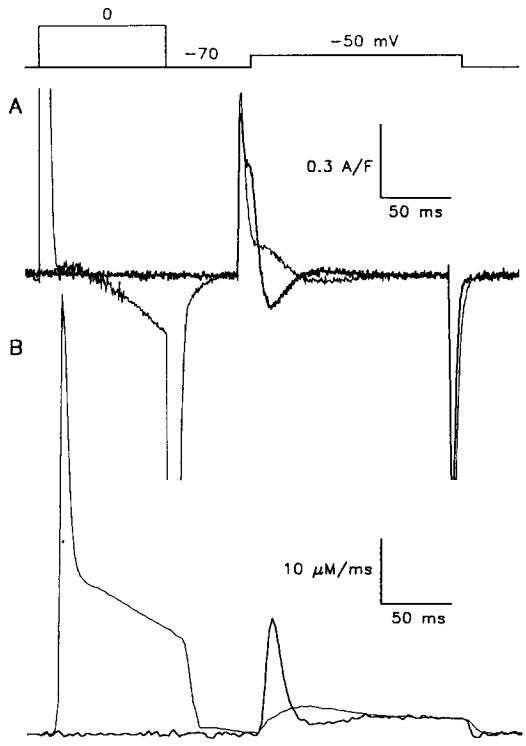


FIGURE 14. Effects of conditioning on the delayed components of $I_Q$. Voltage protocols are schematic. (*A*) Superimposed traces of $I_Q$ (asymmetric current minus steady level at end of pulse) elicited by the pulse protocol with (*thin line*) or without a 90-ms conditioning pulse to 0 mV. (*B*) Release fluxes calculated from the $Ca^{2+}$ signals simultaneously measured with the current records on *A*. Fiber: #1072; diameter: 101.2 μm; linear capacitance: 15 nF; holding potential: −90 mV. Parameters of removal: [EGTA], 7.5 mM; $k_{ON\ Ca\ EGTA}$, 1.5 $\mu M^{-1}\ s^{-1}$; $k_{OFF\ Ca\ EGTA}$, 6.0 $s^{-1}$; maximum pump rate; 1.5 mM $s^{-1}$.

A second intervention was the intracellular application of the fast $Ca^{2+}$ buffer BAPTA, reported to reduce the $I_\gamma$ and Ca release flux (González and Ríos, 1992, 1993; Polakova and Heiny, 1994). Our aim here was to see whether the effect was extensive to the later phases of $I_Q$. Shown in Fig. 15 are the asymmetric current (*A, top*) and $Ca^{2+}$ transient (*B* ), measured simultaneously in 10 EGTA internal solution. Then the solution was changed to one with 20 mM BAPTA and no added $Ca^{2+}$. After 30 min (*bottom*) the $Ca^{2+}$ transient was 20-fold smaller (*B*) and the delayed components of the asymmetric current were essentially eliminated (*A*). In other experiments (González and Ríos, 1992) the effects of BAPTA have been found to be slowly reversible. Even though the mechanism of the effect may be complex (Polakova and Heiny, 1994), it is clear in these records that the buffer selectively

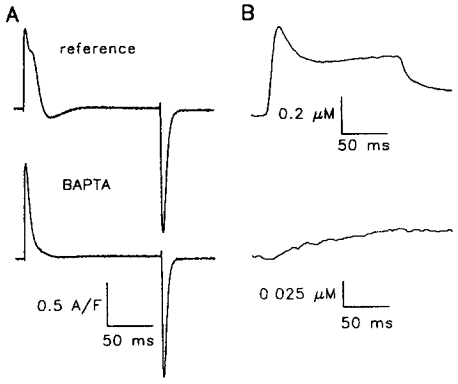


FIGURE 15. Elimination of the late phases by BAPTA. (*A*) Charge movement recorded at pulse from −60 to −35 mV in 10 EGTA internal solution (reference) and 30 min after change to a solution with BAPTA. B. $Ca^{2+}$ transients recorded simultaneously with the current records in *A*. Fiber: #1067; diameter: 113.1 μm; linear capacitance: 16.5 nF. The composition of the internal solution with BAPTA was (in millimolar): ApIII, 0.8; ATP, 5; BAPTA, 20; Cs, 145; Glucose, 5; Glutamate, 60; Hepes, 10; Mg, 5.5; Phosphocreatine, 5. The pH was set to 7.0 at room temperature, no $Ca^{2+}$ was added.

reduced all three delayed phases of charge movement, as it reduced the $Ca^{2+}$ transient.

Finally, we applied interventions to block the $Ca^{2+}$ release channels. It has been reported that ruthenium red (Csernoch et al., 1991) and 1-octanol (González, Pizarro, Ma, Caputo, and Ríos, 1990) partially or totally suppress $Ca^{2+}$ release and reduce or eliminate hump component and inward phase of $I_Q$. Similar results were obtained by García, Avila-Sakar, and Stefani (1991) with ryanodine. In the same group of interventions we may include the phosphatase butanedione monoxime (De Armas, González, Pizarro, and Brum, 1993) and tetracaine (Csernoch et al., 1991; Pizarro, Csernoch, Uribe, and Ríos, 1992), although the mechanism of their action may be more complex than that of ryanodine.

We tested the effects of ryanodine, presumably the most specific of the above-mentioned drugs, on the phases of $I_Q$. Fig. 16 demonstrates the effect of 20 μM ryanodine (a concentration that blocks release channels, reviewed by Lai and Meissner, 1989), added to the external 10 Ca solution. After a brief phase of potentiation (García et al., 1991, not shown) the drug progressively reduced the release flux and $Ca^{2+}$ transients. The changes in $I_Q$ included reduction or elimination of all delayed phases (*A*).

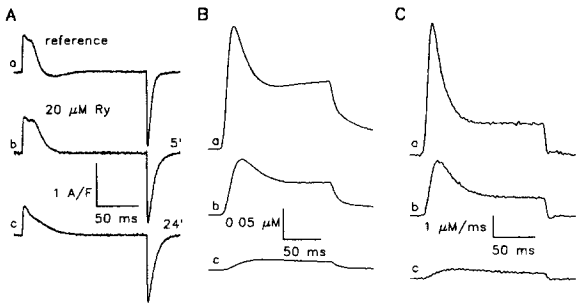


FIGURE 16. Ryanodine suppresses the oscillations. (*A*) Charge movement for a pulse from −90 to −50 mV measured in 10 Ca (*a*) and 5 (*b*) or 24 min (*c*) after adding 20 μM ryanodine extracellularly. (*B*) Ca $^{2+}$ transients recorded simultaneously with the charge movement in *A*. (*C*) Release fluxes calculated from the $Ca^{2+}$ signals. Fiber: #1187; diameter: 96.2 μm; linear capacitance: 21 nF. Parameters of removal: [EGTA], 10 mM; $k_{ON\ Ca\ EGTA}$, 0.7 $\mu M^{-1}\ s^{-1}$; $k_{OFF\ Ca\ EGTA}$, 3.4 $s^{-1}$; maximum pump rate, 1 mM $s^{-1}$.

In summary, even though the "oscillations" in asymmetric current were very resistant to ionic changes in the internal and the external solutions, some of which altered substantially the cable properties of the fiber, they were very sensitive to pulse patterns and other interventions intended to affect primarily the release flux.

## DISCUSSION

The present results confirm the observation of an inward phase in asymmetric currents measured in conditions that should block ionic currents, and demonstrate a later outward phase in the asymmetric current. Various pulse patterns and interventions, designed to distinguish between a capacitive and a conductive mechanism for these components, gave results consistent with a capacitive mechanism. All the phases of the asymmetric current appear to be intramembranous charge movement.

The many results are difficult to reconcile with any major ionic contribution to the inward phase. Thus, the equality between ON and OFF was satisfied for all durations and patterns, and the OFF charge transfer when repolarization intersected the peak inward phase was independent of the OFF potential. As argued many times before, it is essentially impossible to maintain this equality at different voltages and durations in the presence of any appreciable ionic current. The inward phase was visible in a narrow range of voltages. This argues against the voltage-dependent (or $Ca^{2+}$-dependent) activation of outward currents, as such mechanism predicts continued increase and speeding of the currents as $V$ increases. Moreover, the composition of internal and external solutions essentially precluded a contribution to the currents by any of the major permeant ions. Most significantly, large increases in intracellular [$Cl^-$] had no major effects on the various phases, even when increasing the holding current greatly. Nor did the use of $Ca^{2+}$-free external solutions, and of extracellular cations that block $Ca^{2+}$ channels, prevent the occurrence of delayed phases.

Given the theoretical significance of an inward phase in intramembranous charge movement, and the opposite conclusion by Hui and Chen (1994) on the nature of the inward phase, we considered other explanations. For example, it is at least conceivable that the phases in the current are the consequence of an imperfect control of transmembrane voltage, with time-dependent errors that could be described as an oscillation of the clamp. To begin with, the "oscillation" would have to be restricted to the ON of the pulses, since we never observed comparable phases in charge movement during the OFF. However, one could still speculate that a $Ca^{2+}$-dependent change in cable properties causes oscillations or clamp errors restricted to the ON. The direct measurement of intracellular potential illustrated in Fig. 2 shows, however, that there are no major errors in potential, nor obvious asymmetries between ON and OFF. Moreover, the fact that the inward and second outward phases were still there in an internal solution with 50 mM $Cl^-$, even though the resting membrane current and the capacitance in control pulses were changed, indicates that changes in cable properties of an even greater magnitude would be necessary to affect these phases substantially. Finally, we have observed similar phases in the current using a four Vaseline-gap device (Ríos et al., 1989) in which the regions under the seals are guarded, and well polarized, which rules out those regions as source of oscillations. All the evidence indicates that voltage clamp inhomogeneities are not the cause of the delayed phases in the asymmetric current.

In contrast with the insensitivity of these phases to changes in internal or external ionic composition, they were profoundly altered by different interventions intended to affect primarily the release flux. One must conclude that these phases of asymmetric current were intramembranous charge movements, linked to $Ca^{2+}$ release.

The three phases of the delayed charge movement, hump, inward phase and second outward, followed one another with decreasing amplitude and increasing duration. At least in a descriptive sense, they constitute a damped oscillation. As remarked in the Introduction, the importance of such an oscillation in charge movement cannot be overstated, it requires a fluctuation in transmembrane voltage. $dV_m/dt$ has to become negative at some point.

Pizarro et al. (1991) presented a detailed model in which the hump and inward phase of asymmetric current were determined by changes in the local transmembrane potential, near the voltage sensor of EC coupling. In turn these changes in potential were pictured as due to binding of $Ca^{2+}$ to specific sites near the voltage sensors. The theory was shown to reproduce various aspects of the charge movement records, when the simulations started from the $Ca^{2+}$ release fluxes derived from the experiments.

If the simulations of Pizarro et al. (1991) are repeated, but using the release fluxes of the present series of experiments, which have a second rising phase, the simulated charge movement currents have, as one would expect, small and slow second outward phases, with features similar to those observed. These simulations, not shown, indicate that the mechanisms underlying all three delayed phases are probably related.

### *A Comprehensive Model of Feedback in EC Coupling*

A different, more radical approach to modeling these phenomena proved to be more rewarding. We have argued before that a mechanism like the one proposed by Pizarro et al. (1991), in which the increase in $[Ca^{2+}]_i$ due to $Ca^{2+}$ release increases locally the transmembrane potential, constitutes a positive feedback interaction, by which release is capable of self-reinforcing, via the effects of $Ca^{2+}$ on the voltage sensors. By the same token, an inactivation of release by $Ca^{2+}$, as proposed by Schneider and Simon (1988), would constitute a negative feedback influence. One possible interpretation of the three delayed phases in charge movement would be that the concurrence of positive and negative feedbacks may result in an oscillation of the entire system.

Fig. 17 illustrates how such an oscillation could arise: depolarization by a small suprathreshold pulse first results in the activation of some voltage sensors which in turn activate some release channels. The ensuing increase in $[Ca^{2+}]_i$ near the triads results in local voltage increase and further activation of voltage sensors and their associated channels, the positive feedback. Together with the greater activation and peak of release comes the inactivation process, presumably by $Ca^{2+}$, leading to the decay in release flux and a consequent decay in the local $[Ca^{2+}]_i$ and local voltage (especially if high EGTA is present). This gives rise to the return of some voltage sensors from the activating states (the inward phase of charge movement) and further release channel closure. The reduction in local $Ca^{2+}$ then gives the opportunity for

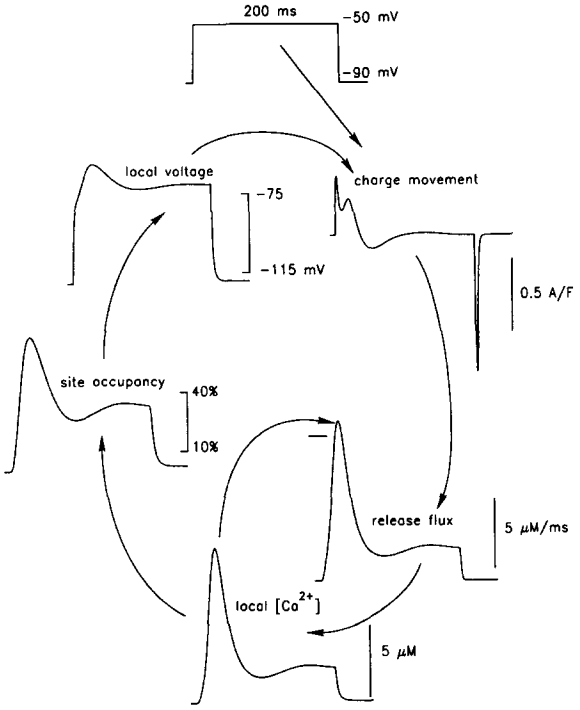


FIGURE 17. Logic and sequence of calculations in the EC coupling model. The computations start with the application of a voltage step (with exponential rise of $\tau = 1.5$ ms), then the response of the voltage sensors is computed (Eq. 1, details in Ríos et al., 1993). The movement of charge modifies the state of the release channels, as described by Ríos et al. (1993). The occupancy $P_o$ of the open states is computed, and a flux of release is calculated, proportional to $P_o$ and to the calcium content of the SR. The diffusion and binding equations of Pizarro et al. (1991) are then used to calculate a local $[Ca^{2+}]_i$. This $[Ca^{2+}]_i$ drives two binding reactions, to the inhibitory site on the release channel (Eq. 2) and to the site $S$, that determines $I\gamma$ (Eq. 3). The program then calculates the redistribution of $Ca^{2+}$-bound release channels between open and inactivated states (inactivation is not assumed to have any consequences on the allosterically coupled voltage sensors). The occupancy of $S$ is used to calculate a new value for the local transmembrane potential, and the cycle of calculations restarts with the modified membrane potential. The calculations were performed by the method of Euler with a 1 or 0.5-μs increment, with no difference in the results. The program produces as output the waveforms illustrated, plus many others not shown, including distribution of free and bound $Ca^{2+}$ and $Ca^{2+}$ ligands in every slice of the sarcomere. Parameters of the voltage sensor. $\bar{V}$, −25 mV; $K$, 4.5 mV, corresponding to an apparent valence of 1.3 per particle; α, 0.5 $ms^{-1}$; $Q_{max}$, 20 nC/μF. Parameters of the release channel: $k_L$, 0.005 $ms^{-1}$; $k_{L^-}$, 1,800 $ms^{-1}$; $f$, 0.15; initial [Ca] in SR, referred to accessible myoplasmic volume, 5 mM; $R_{max}$, maximum possible release flux (when $P_o = 1$ and SR content = 5 mM), 90 mM $s^{-1}$. Parameters of inactivation: $K_r$, 5 μM; $k_i$, 70 $s^{-1}$; $k_r$, 6 $s^{-1}$. Parameters of the γ site: $V_{max}$, −30 mV; $k_s$, 200 $\mu M^{-1}\ s^{-1}$; $k_s^-$, 1,000 $s^{-1}$. The diffusion coefficients were assigned as follows: for $Ca^{2+}$ a value of $2.8 \times 10^{-6}$ $cm^2/s$, which is 2.5-fold smaller than its value in water (Kushmerick and Podolsky, 1969); for ApIII the value $3.6 \times 10^{-7}$ $cm^2/s$ (estimated by Kovacs et al., 1983) and for EGTA, $10^{-6}$ $cm^2/s$ (Pizarro et al., 1991). The values of the removal parameters are listed in Methods.

some release channels to recover from inactivation and the system may swing back into activation.

To test whether the processes described and what is known about their quantitative aspects can account quantitatively for the observations, we constructed a mathematical model of EC coupling, using for each process the consensual quantitative formulation, or one that we favored where there was no consensus. The model includes the following elements.

*The voltage sensors.* Voltage sensors are represented (Ríos et al., 1993) as four identical two-state particles, moving under the influence of the local transmembrane potential. The kinetics of the transitions are described by exponential rate constants that assume a symmetric barrier:

$$k_C = 0.5\ \alpha e^{(V-\bar{V})/8K}$$

$$k_C^- = 0.5\ \alpha e^{-(V-\bar{V})/8K} \quad (1)$$

Three parameters describe this movement: a transition voltage $\bar{V}$, a steepness factor $4K$ (equal to $RT/zF$, where $R$ is the gas constant, $T$ the temperature, $z$ the effective valence of the particle and $F$ the faraday), and a rate parameter $\alpha$, equal to the rate constant of the exponential relaxation at the transition potential. The movement of charge is initially driven by the "macroscopic" change in membrane potential, which is described by a pulse with exponential edges of time constant 1.5 ms. The membrane is considered to be homogeneously polarized at all times.

*The release channels.* Release channels are activated by the voltage sensors exclusively (in other words, the present model does not have $Ca^{2+}$-dependent activation of release). The formulation used to represent the activation of release by the sensors is the allosteric model of Ríos et al. (1993). In this formulation, the interaction is described by just one parameter, the allosteric factor $f$ ($< 1$), and for every sensor particle that moves to the activating state, the forward and (backward) rate constants of release channel opening, $k_L$ and ($k_L^-$), are multiplied (divided) by $1/f$. The allosteric formulation is not critical to the present model, however; very similar results are obtained if the activation of channel opening is made simply proportional to a power of the charge transferred (a Hodgkin-Huxley $m^3$ or $m^4$ model, as proposed by Simon and Hill, 1992). Release flux was made proportional to the occupancy of the open states ($P_o$), and to the total Ca content in the SR, which was computed simply as the difference between an initial value and the amount released (the flux of uptake by the pump was not included in the short term material balance of the SR, as it is not clear whether this $Ca^{2+}$ becomes immediately available for release).

*Ca-dependent inactivation.* Once the release channels open, $Ca^{2+}$ is released and its concentration increases locally. Following a formulation of Simon et al. (1991) the release channels (or receptors, $R$, associated to the channels) bind two $Ca^{2+}$ in a rapidly equilibrating reaction, and the $Ca^{2+}$-bound channels inactivate more slowly to a closed state $R^*$

$$2Ca + R \overset{K_r}{\rightleftarrows} Ca_2R \underset{k_r}{\overset{k_i}{\rightleftharpoons}} Ca_2R^* \quad (2)$$

*Local transmembrane potential.* A key aspect of the model is the existence of $Ca^{2+}$ binding sites (the "γ sites," $S$), at or near the inner face of the voltage sensors. These are treated, as done by Pizarro et al. (1991), with the reaction scheme

$$S + Ca \underset{k_s}{\overset{k_s}{\rightleftharpoons}} SCa. \quad (3)$$

Changes in local $[Ca^{2+}]_i$ result in changes in saturation of the sites, which are assumed to be rapidly equilibrating. The free sites make a negative contribution, $V_{max}$, to the transmembrane potential, and complete saturation by $Ca^{2+}$ reduces this contribution to 0.

*Diffusion, binding, and removal of $Ca^{2+}$ in the sarcomere.* The myoplasmic space is treated as a discrete set of homogeneous compartments, arranged linearly, 18 per sarcomere (Pizarro et al., [1991] described in detail in their Appendix II). The released $Ca^{2+}$ is put symmetrically in the first and last of these compartments, then diffuses along the sarcomere towards the center. As it diffuses, it binds to diffusible ligands (representing parvalbumin and the extrinsic buffers, including the dye), to fixed sites (representing troponin and pump sites), and it is transported into the SR. The diffusion/binding equations of the model are solved ($Ca^{2+}$, ApIII and EGTA are allowed to diffuse, whether parvalbumin diffuses or not had no detectable effect in the simulations), and the $[Ca^{2+}](t)$ is obtained in every one of the 18 "slices" along the sarcomere. In particular the local concentration at the triad (first slice) is used to

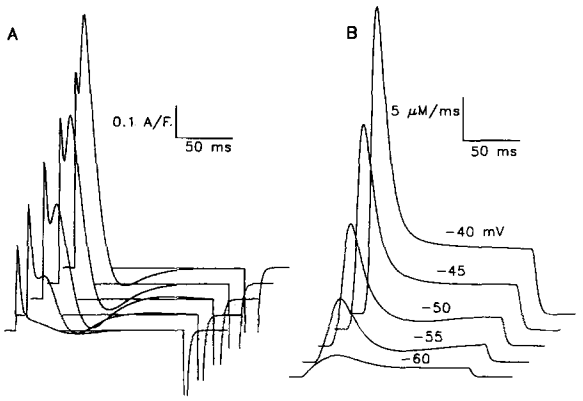


FIGURE 18. Time course of simulated records at different potentials. See description in previous figure. Parameter values are as given there, except for the following: $R_{max}$, 120 mM $s^1$; $k_i$, 140 $s^{-1}$; $k_r$, 5 $s^{-1}$.

drive binding to the $Q\gamma$ sites, and to the sites responsible for inactivation of the release channel.

The formulation requires the assignment of values to many parameters. This was done in two different ways. For a first set of simulations illustrating general properties of the model, and represented in Figs. 17–19, we used a set of generic values of the parameters, listed in the legend of Fig. 17. Then we attempted to fit in detail all the records in a specific experiment (Fig. 20). For that purpose the procedure and parameter set was modified somewhat, as described later.

The numerical solutions of the system of equations include the waveforms of all the measured variables. Fig. 17 illustrates the logic of the computations and presents simulated records. The input to the computational program is the applied voltage pulse, (*top*). It can be seen that the model produces charge movement currents with hump, inward and second outward phase, and that it also produces release records with a second rising phase, qualitatively similar to the experimental ones.

In Fig. 18 are a series of simulations with the same parameters at different voltages.

Comparing this with the family of records in Fig. 12, it can be seen that the simulations reproduce well the fact that the amplitude of the inward phase in $I_Q$ reaches a maximum at slightly suprathreshold voltages (−50 in the simulations), and that the presence and size of the second outward phase corresponds well with the second rising phase in release flux.

Fig. 19 represents simulated records of release flux, $I_Q$ and the derivative $\dot{R}(t)$. The timing relationships observed experimentally are well simulated, including the cotemporality of the apex of the hump and the maximum of $\dot{R}((t)$, the earlier and more marked negative extreme in $\dot{R}(t)$, and the rough coincidence in time of the late positive phases. It is apparent, however, that the late outward phase of $\dot{R}(t)$ precedes the corresponding phase in $I_Q$, a dissociation that was not obvious in the experiments (Fig. 12).

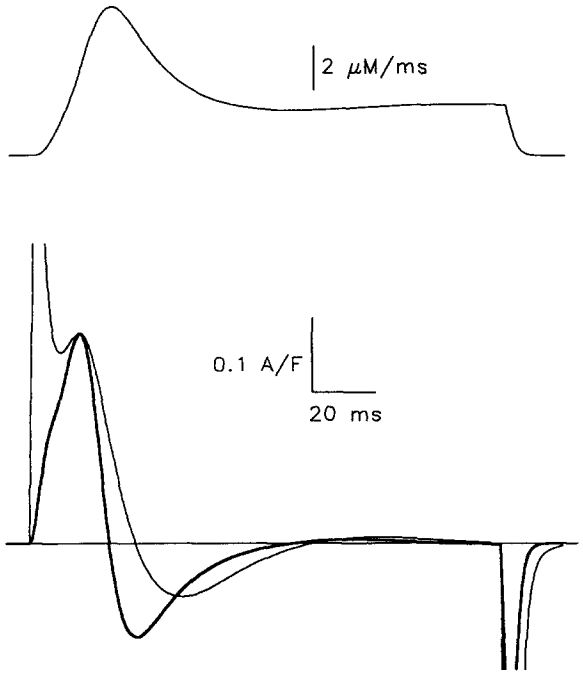


FIGURE 19. Timing relationships in the simulations. (*Top*) Simulated release flux for a −55 mV pulse (from −90 mV). (*Bottom*) Simulated charge movement record and time derivative of release flux, scaled to match its peak with the hump of charge movement. Same parameter values as in Fig. 17, except for the following: $k_i$, 90 $s^{-1}$; $k_r$, 8 $s^{-1}$; $V_{max}$, −25 mV.

Finally, Fig. 20 compares simulated waveforms with records from an actual experiment. The experimental records were quite well reproduced, but two changes were needed: we used the generalized allosteric model of Ríos et al. (1993) in which the voltage sensor molecules have multiple charged particles (as in their work, two particles per sensor reproduced the results better than one, and more particles did not improve the fit). Also, instead of the generic set of values of removal parameters listed in Methods, we used the specific values fitted to the $Ca^{2+}$ transients of this particular fiber (listed in the figure legend). In general, the agreement is remarkably good; the simulations reproduce the oscillations in quantitative, as well as qualitative detail.

The simulations are robust: their qualitative aspects are not sensitive to the particular choice of parameter values, within broad ranges. We already indicated that a Hodgkin-Huxley formulation of coupling between sensors and channels can replace the allosteric model formulation, giving similar results. The simulations were also insensitive to details of the removal system, provided that the removal formulations described well the decay of the experimental $Ca^{2+}$ transients. For instance, we did not find major changes in the simulated waveforms when we formulated the rate of transfer of $Ca^{2+}$ into the SR as proportional to either the first, the second or the fourth power of the occupancy by $Ca^{2+}$ of the pump binding sites. Also, without major consequences was the use of the 11-stage pump model of Fernández-Belda, Kurzmack, and Inesi (1989), with parameter values used in the same work, and rate

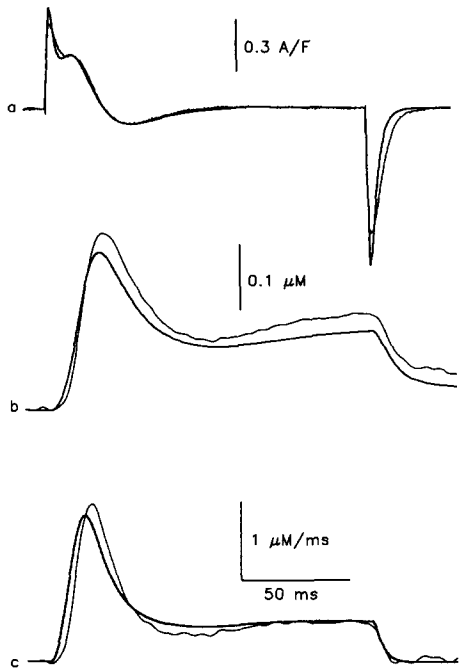


FIGURE 20. Comparison between simulations and experimental records. Simultaneously obtained experimental records of charge movement (*top*), $\Delta[Ca^{2+}](t)$ (*middle*) and the experimentally derived release flux, for a pulse to −45 mV from a prepulse level of −70 mV. The experiment is # 1056, the same as in Figs. 12 and 13. The smooth records are simulations with a single set of parameters. The simulations used the generalization of the allosteric model of Ríos et al. (1993) with two charged particles per voltage sensor. The following parameter values were different than in the simulations of Fig. 17: $f$, 0.22; $k_i$, 200 $s^{-1}$; $R_{max}$, 55 mM $s^{-1}$. The removal parameters were set at the values found by fitting the experimental $Ca^{2+}$ transients (Fig. 12, *legend*).

constants corrected to the temperature of the present experiments with a $Q_{10}$ of 3 (and initial conditions for a resting $[Ca^{2+}]_i$ of 20 nM, kindly supplied to us by S.M. Baylor, University of Pennsylvania).

The parameters that really influence the results, determining for instance whether there are three delayed phases in charge movement, are the size of the inactivating portion of release (determined chiefly by the ratio of the inactivation rate constants and the affinity for $Ca^{2+}$ of the inactivation site), and the magnitude of $V_{max}$ (which determines the size of the hump and related phases of $I_\gamma$ ).

Another important factor is EGTA. Experimentally, the most marked inward phases are seen in slack fibers in high [EGTA] (although we cannot tell whether EGTA or the fact that the fibers are slack is more important). It was using a high

EGTA solution that Pizarro et al. (1991) recorded the inward phases that motivated their initial report. By contrast, inward phases were absent or small, and dismissed as an effect of time-dependent ionic currents, in the previous work with unbuffered internal solutions (Ríos and Brum, 1987; Csernoch et al., 1991; Szucs et al., 1991).

Fig. 21 demonstrates the effect of EGTA in the model. The top records are simulated charge movement currents, using the standard parameters, with either 10 mM of the ligand representing EGTA (*continuous line*) or 0.001 mM (*dotted*). In the simulations, the presence of EGTA helps reduce rapidly the local $[Ca^{2+}]_i$ after the peak of $\dot{R}(t)$, thus, driving the unbinding of $Ca^{2+}$ from the hypothetical sites, which in turn causes the inward movement of intramembranous charge.

The simulations without EGTA help understand another discrepancy with previous results. In some of the previous reports, chiefly that by Szucs et al. (1991), the $I_\gamma$ humps were accompanied by an excess of ON over OFF charge transfer. In the present experiments that difference does not exist (provided that pulses longer than 150 ms are used, as in Figs. 3 and 7). This is also the case in the simulations. The

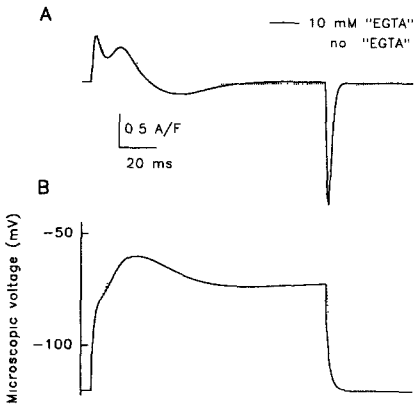


FIGURE 21. Effects of EGTA in the simulations. (*A*) Charge movement current elicited by a pulse to −50 mV. Parameter values were similar to those listed in Fig. 17, except for [EGTA], that was either 10 mM (*solid line*) or 0.001 mM (*dotted line*). The ON and OFF rate constants of Ca:EGTA were 1 $\mu M^{-1}$ $s^{-1}$ and 1 $s^{-1}$. (*B*) Corresponding microscopic transmembrane potential difference.

microscopic transmembrane potential (Fig. 21 *B*), which in the model has a contribution from time-varying occupancy of $Ca^{2+}$ sites, returns abruptly to the resting level in the presence of EGTA (Fig. 21, *solid line*) but stays elevated in its absence, and only slowly returns to the resting level as $Ca^{2+}$ is taken away by the removal elements of the model. This predicts that in an experiment part of the charge transferred during the ON will return slowly at the OFF, and be lost by the conventional integration used for instance by Szucs et al. (1991). The discrepancy is made worse if pulses of 100 ms or shorter are used, because in this case the ON charge transfer is computed from a baseline that may be shifted negatively by a slow and small inward phase of charge movement. This causes $Q_{ON}$ to be overestimated.

There are discrepancies between results and simulations in two main aspects. The simulated $I_Q$ is in good temporal agreement with the experiment during the ON if charge movement is made intrinsically very fast (quantified by the parameter $\alpha$, which was 0.5 $ms^{-1}$ in the simulations). Because this is faster than the measured rate constants ($\alpha$ should be equal to the rate constant at the transition voltage) the

simulated charge movement is too fast during the OFF. This problem was already noted by Pizarro et al. (1991), who suggested as an explanation that the intrinsic speed of charge movement could be faster than the rate measured in voltage clamp experiments, presumably limited by lags in polarization of the *T* tubule.

Another problem is that the simulations that imitated well the initial phases of the oscillation had a comparatively small second outward phase in $I_Q$ and secondary rise in $\dot{R}(t)$. Even though we did not exhaust the possible combinations of parameter values (because every run of simulations, for one set of values, takes some 5 min of computer time), we are quite confident that this is a basic property of the model, it does oscillate less than the real data. One explanation may be that inactivation is treated as dependent on "bulk" triadic calcium, when the reality could be quite different. Indeed, the simulations simplify the issue of diffusion to a one-dimensional situation. This lumps the whole triadic region of the cytoplasm into one homogeneous slice, overlooking the existence of transversal gradients.

There are increasing indications of the existence of large $Ca^{2+}$ gradients inside skeletal muscle cells, including what appears to be the first successful measurement of such gradients (Escobar and Vergara, 1993). Not surprisingly, lumped models lead to inconsistencies. For example, Hill and Simon (1991) could not elicit inactivation in skeletal fibers using photorelease techniques that increased the $[Ca^{2+}]_i$ way above the estimates of dissociation constant of the inactivation site (300 nM, Schneider and Simon, 1988) which were derived using a lumped model. The present simulations, by allowing for longitudinal gradients (along the sarcomere), solve the inconsistencies to some extent; thus, a value of 5 μM was found suitable for $K_r$, already more than one order of magnitude greater than the estimate with the lumped model. It is likely that the phenomenon depends on still higher $[Ca^{2+}]_i$, present near the mouth of the open channel. Some evidence in this direction has been found recently (Pizarro and Ríos, 1994).

This model does not explain the absence, or very small magnitude of $I\gamma$ components observed in many works with stretched fibers (Melzer, Schneider, Simon, and Szucs, 1986; Brum, Fitts, Pizarro and Ríos, 1988*b*; Simon and Hill, 1992). The main difference with the conditions of the present experiments was stretch (to beyond 4 μm/sarcomere in the work of Brum et al., 1988*b*). A speculation is that extreme stretching causes alterations, possibly in the geometry of the membrane systems, leading to a reduction in $I_\gamma$. It is not clear that stretch is the only cause of the reduction of $I\gamma$ in those experiments, as Hui (1991) found no effects on $I\gamma$ of stretching frog fibers from 3.5 to 4.0 μm/sarcomere.

### *A Putative Ca-binding Site on the Internal Face of the Voltage Sensor*

Since the present results make a strong case for $Ca^{2+}$ binding on or near the voltage sensor, it is interesting that a cytoplasmic stretch of 27 aminoacid residues in the $\alpha_1$ subunit has been identified as a putative $Ca^{2+}$-binding site (Babitch, 1990). This stretch starts at E1401, that is, 18 residues downstream of the COOH-terminal (intracellular) end of transmembrane segment 6 in domain IV. It is probably a $Ca^{2+}$ binding site as it fulfills most of the criteria for an EF-hand (Kretsinger, 1975, 1987; Tufty and Kretsinger, 1975). It is highly conserved, being present in the rabbit $\alpha_1$ and in the corresponding protein from carp, as well as in the rat cardiac channel. It

should be very similar in the frog. In our model, we require the γ site to be punctual rather than widespread (so as not to charge extensive areas of the membrane when its potential changes), and to be located near the moving intramembranous charge, but without being a part of it. The location of the near-EF-hand is precisely as required. Finally, the model consistently requires a site of moderate affinity, with a $K_D$ of 10 or 20 μM. The putative site is not an EF-hand. It matches EF-hand criteria at 14 of 16 specified locations (a "Tufty-Kretsinger score" of 14 out of 16); the two misses are at two of the seven coordination sites (locations $Z$ and $-X$; Kretsinger, 1975), where the stretch has lysines instead of oxygen-bearing side chains. These are important mismatches; they are unlikely to destroy the $Ca^{2+}$-binding character, as there are other proteins with two or more positive residues within the binding fold (like vitamin D-dependent intestinal $Ca^{2+}$-binding protein and its homologs [Kretsinger, 1987; Szebenyi and Moffat, 1986]), but the affinity may be much lower than that of typical EF-hand proteins. If this site had 1000-fold less affinity than, say, parvalbumin, its $K_D$ would be 10 μM, the value required in the simulations.

We thank Dr. R. Shirokov for help in performing measurements of transmembrane voltage, Dr. A. González, for allowing us to use data from an experiment on the effects of BAPTA, and Dr. S. Baylor for providing the set of initial conditions used in simulations with the SR pump model of Fernández-Belda et al. (1984).

This work was supported by the United States Public Health Service, National Institute of Arthritis and Musculoskeletal and Skin Diseases grant AR-32808.

*Original version received 9 December 1993 and accepted version received 21 March 1994.*

## REFERENCES

Adrian, R. H., and A. Peres. 1977. A gating signal for the potassium channels? *Nature.* 267:800–804.

Babitch, J. 1990. Channel hands. *Nature.* 346:321–322.

Brum, G., E. Ríos, and E. Stefani. 1988*a*. Effects of extracellular calcium calcium on the calcium movements of excitation-contraction coupling in skeletal muscle fibers. (Appendix by Brum, G., E. Ríos, and M. F. Schneider. *Journal of Physiology.* 398:441–473.

Brum, G., R. Fitts, G. Pizarro, and E. Ríos. 1988*b*. Voltage sensors of the frog skeletal muscle membrane require calcium to function in excitation-contraction coupling. *Journal of Physiology.* 398:475–505.

Chen, W., and C. S. Hui. 1991. Gluconate suppresses Qβ more effectively than Qγ in frog cut twitch fibers. *Biophysical Journal.* 59:543*a*. (Abstr.)

Csernoch, L., G. Pizarro, I. Uribe, M. Rodríges, and E. Ríos. 1991. Interfering with calcium release suppresses the "hump" component of intramembranous charge movement in skeletal muscle. *Journal of General Physiology.* 97:845–884.

De Armas, R., S. González, G. Pizarro, and G. Brum. 1993. BDM suppresses calcium release and Qγ in skeletal muscle fiber. *Biophysical Journal.* 64:A240. (Abstr.)

Escobar, A., and J. Vergara. 1993. Confocal spot detection of $Ca^{2+}$ transients in a single sarcomere of skeletal muscle fibers. *Biophysical Journal.* 64:A241. (Abstr.)

Francini, F., and E. Stefani. 1989. Decay of slow calcium current in twitch muscle fibers of the frog is influenced by intracellular EGTA. *Journal of General Physiology.* 94:953–969.

Fernández-Belda, F., M. Kurzmack, and G. Inesi. 1984. A comparative study of calcium transients by isotopic tracer, metallochromic indicator, and intrinsic fluorescence in sarcoplasmic reticulum ATPase. *Journal of Biological Chemistry.* 259:9687–9698.

García, J., A. J. Avila-Sakar, and E. Stefani. 1991. Differential effects of ryanodine and tetracaine on charge movement and calcium transients in frog skeletal muscle. *Journal of Physiology.* 440:403–417.

García, J., G. Pizarro, E. Ríos, and E. Stefani. 1991. Effect of the calcium buffer EGTA on the "hump" component of charge movement in skeletal muscle. *Journal of General Physiology.* 97:885–896.

González, A., G. Pizarro, J. Ma, C. Caputo, and E. Ríos. 1990. Effects of 1-alkanols on E-C coupling. *Biophysical Journal.* 57:A341. (Abstr.)

González, A., and E. Ríos. 1992. Reversible abolition of Qγ by intracellular BAPTA in frog muscle. *Biophysical Journal.* 61:A130. (Abstr.)

González, A., and E. Ríos. 1993. Perchlorate enhances transmission in skeletal muscle excitation-contraction coupling. *Journal of General Physiology.* 102:373–421.

Heiny, J., D. Jong, S. H. Bryant, D. Conte-Camerino, and V. Tortorella. 1990. Enantiomeric effects on charge movement and mechanical threshold in frog skeletal muscle by a chiral clofibric acid analog. *Biophysical Journal.* 57:147–152.

Hill, D., and B. Simon. 1991. Use of "caged calcium" in skeletal muscle to study calcium-dependent inactivation of SR calcium release. *Biophysical Journal.* 59:A239. (Abstr.)

Huang, C. L. H. 1989. Intramembrane charge movements in skeletal muscle. *Physiological Reviews.* 68:1197–1247.

Hui, C. S. 1991. Comparison of charge movement components in intact and cut twitch fibers of the frog. Effects of stretch and temperature. *Journal of General Physiology.* 98:287–314.

Hui, C. S., and W. Chen. 1992. Effect of conditioning depolarization and repetitive stimulation on Qβ and Qγ charge components in frog cut twitch fibers. *Journal of General Physiology.* 99:1017–1043.

Hui, C. S., and W. Chen. 1994. Evidence for the non-existence of a negative phase in the hump charge movement component (Iγ) in *Rana temporaria*. *The Journal of Physiology.* 474:275–282.

Irving, M., J. Maylie, N. L. Sizto, and W. K. Chandler. 1987. Intrinsic optical and passive electrical properties of cut frog twitch fibers. *Journal of General Physiology.* 89:1–41.

Jong, D.-S., P. C. Pape, and W. K. Chandler. 1992. Effects of sarcoplasmic reticulum (SR) calcium depletion on intramembranous charge movement in frog cut muscle fiber. *Biophysical Journal.* 61:A131 (Abstr.)

Kovács, L., E. Ríos, and M. F. Schneider. 1983. Measurement and modification of free calcium transients in frog skeletal muscle fibers by metallochromic indicator dye. *Journal of Physiology.* 343:161–196.

Kretsinger, R. H. 1975. Hypothesis: calcium modulated proteins contain EF-hands. *In* Calcium Transport in Contraction and Secretion. E. Carafoli, F. Clementie, W. Drabikowski, and A. Magreth, editors. North-Holland Publishing, Amsterdam. 469–478.

Kretsinger, R. H. 1987. Calcium coordination and the calmodulin fold: divergent versus convergent evolution. *Cold Spring Harbor Symposia on Quantitative Biology.* 52:499–510.

Kushmerick, M. J., and R. J. Podolsky. 1969. Ionic mobility in muscle cells. *Science.* 166:1297–1298.

Lai, F. A., and G. Meissner. 1989. The muscle ryanodine receptor and its intrinsic $Ca^{2+}$ channel activity. *Journal of Bioenergetics and Biomembranes.* 21:227–246.

Melzer, W., E. Ríos, and M. F. Schneider. 1984. Time course of calcium release and removal in skeletal muscle fibers. *Biophysical Journal.* 45:637–641.

Melzer, W., M. F. Schneider, B. J. Simon, and G. Szucs. 1986. Intramembrane charge movement and calcium release in frog skeletal muscle. *Journal of Physiology.* 373:481–511.

Pape, P. C., D.-S. Jong, and W. K. Chandler. 1992. Effects of sarcoplasmic reticulum (SR) calcium loading on intramembranous charge movement in frog cut muscle fibers. *Biophysical Journal.* 61:A130. (Abstr.)

Pizarro, G., L. Csernoch, I. Uribe, M. Rodríguez, and E. Ríos. 1991. The relationship between Qγ and Ca release from the sarcoplasmic reticulum in skeletal muscle. *Journal of General Physiology.* 97:913–947.

Pizarro, G., L. Csernoch, I. Uribe, and E. Ríos. 1992. Differential effects of tetracaine on two kinetic components of calcium release in frog skeletal muscle fibers. *Journal of Physiology.* 457:525–538.

Pizarro, G., and E. Ríos. 1994. Simon's paradox. Local inactivation of Ca release in skeletal muscle. *Biophysical Journal.* 66:A339. (Abstr.)

Polakova, K., and J. A. Heiny. 1994. Effects of intracellular calcium on charge movement in frog skeletal muscle. *Biophysical Journal.* 66:A86 (Abstr.)

Ríos, E., and G. Brum. 1987. Involvement of dihydropyridine receptors in excitation-contraction coupling in skeletal muscle. *Nature.* 325:717–720.

Ríos, E., G. Pizarro, and G. Brum. 1989. A four gap voltage clamp improves measurements of EC coupling events in frog skeletal muscle. *Biophysical Journal.* 55:237*a*. (Abstr.)

Ríos, E., M. Karhanek, J. Ma, and A. González. 1993. An allosteric model of the molecular interactions of excitation-contraction coupling in skeletal muscle. *Journal of General Physiology.* 102:449–481.

Ríos, E., and G. Pizarro. 1991. Voltage sensor of excitation-contraction coupling in skeletal muscle. *Physiological Reviews.* 71:849–908.

Schneider, M. F., and W. K. Chandler. 1973. Voltage dependent charge movement in skeletal muscle: a possible step in excitation-contraction coupling. *Nature.* 242:244–246.

Schneider, M. F., E. Ríos, and W. Melzer. 1987. Determining the rate of calcium release from the sarcoplasmic reticulum in muscle fibers. *Biophysical Journal.* 51:1005–1007.

Schneider, M. F., B. J. Simon, and G. Szucs. 1987. Depletion of calcium from the sarcoplasmic reticulum during calcium release in frog skeletal muscle. *Journal of Physiology.* 392:167–192.

Schneider, M. F., and B. J. Simon. 1988. Inactivation of calcium release from the sarcoplasmic reticulum in frog skeletal muscle. *Journal of Physiology.* 405:727–745.

Simon, B. J., and D. A. Hill. 1992. Charge movement and SR calcium release in frog skeletal muscle can be related by Hodgkin-Huxley model with four gating particles. *Biophysical Journal.* 61:1109–1116.

Simon, B. J., M. G. Klein, and M. F. Shneider. 1991. Calcium dependence of inactivation of calcium release from the sarcoplasmic reticulum in skeletal muscle fibers. *Journal of General Physiology.* 97:437–471.

Szebenyi, D. M. E., and K. Moffat. 1986. The refined structure of vitamin D-dependent calcium-binding protein from bovine intestine. Molecular details, ion binding, and implications for the structure of other calcium-binding proteins. *Journal of Biological Chemistry.* 261:8761–8777.

Szucs, G., L. Csernoch, J. Magyar, and L. Kovács. 1991. Contraction threshold and the "hump" component of charge movement in frog skeletal muscle. *Journal of General Physiology.* 97:897–911.

Tanabe, T., K. G. Beam, J. A. Powell, and S. Numa. 1988. Restoration of excitation-contraction coupling and slow calcium currents in dysgenic muscle by dihydropyridine receptor complementary DNA. *Nature.* 344:134–139.

Tanabe, T., H. Takeshima, A. Mikami, V. Flockerzi, H. Takahashi, K. Kangawa, M. Kojima, H. Matsuo, T. Hirose, and S. Numa. 1987. Primary structure of the receptor for calcium channel blockers from skeletal muscle. *Nature.* 328:313–318.

Tufty, R. M., and R. H. Kretsinger. 1975. Troponin and parvalbumin calcium binding regions predicted in myosin light chain and T7 lysozime. *Science.* 187:167–169.